Polymer Chemistry

ROYAL SOCIETY OF CHEMISTRY

PAPER

View Article Online
View Journal

Cite this: DOI: 10.1039/d6py00380j

Engineering bio-based eutectogels from casein *via* 3D printing

Sebastián Locatelli,[a] Gisela C. Luque,[a,b] Ludmila I. Ronco,[a,c] Oihane Varela,[d] Xabier López de Pariza,[d] David Mecerreyes *[e,f] and Roque J. Minari *[a,c]

Received 16th April 2026,
Accepted 19th June 2026

DOI: 10.1039/d6py00380j

rsc.li/polymers

Eutectogels as an emerging class of soft-ionic materials are gaining attention in bioelectronic applications. Nevertheless, the examples of sustainable eutectogels that can be processed by 3D printing have been limited. Herein, we report the preparation of bio-based eutectogels based on casein and their processing by 3D printing. The eutectogel formulations were based on modified casein (methacrylated casein), poly(ethylene glycol) diacrylate (PEGDA), water, and two natural deep eutectic solvents (DESs) composed of betaine with either glycerol or sucrose. Different PEGDA content and DES types were evaluated to obtain bio-based eutectogels with excellent properties such as high ionic conductivity (up to 1.4 × 10^{-3} S cm^{-1}) and tunable rheological or mechanical properties. The potential of these eutectogels for bioelectronics applications was demonstrated through evaluating their performance as pressure sensors, exhibiting a sensitivity of S = 0.7 kPa^{-1} and stable responses under repeated loading cycles. Finally, the 3D printability of casein-based eutectogels was evaluated in tomographic volumetric additive manufacturing (VAM) and digital light processing (DLP) printing technologies.

1. Introduction

Eutectogels, a type of soft ionic material composed of a polymeric matrix and a deep eutectic solvent (DES), have gained attention due to their advantages over similar gels, such as hydrogels or iongels. These benefits include long-term stability compared to hydrogels, low cost, simple preparation, bio-based character and high ionic conductivity. DESs are liquid eutectic mixtures formed by a hydrogen bond donor (HBD) and a hydrogen bond acceptor (HBA), which interact through hydrogen bonding, resulting in a deviation from the thermodynamic ideality.[1] Over the last few years, eutectogels have been used for different applications, such as battery technologies, CO_2 separation, biocatalysis, drug delivery systems, food packaging, and bioelectronics.[2,3] Especially in bioelectronics, these soft ionic materials find applications as artificial skin, flexible electrodes, wearable biosensors or human–machine interfaces.

In this context, additive manufacturing, commonly known as 3D printing, is a fabrication method that provides precise control over the structure and size of the created object, whereby it is particularly interesting in biomedical applications.[4–6] In recent years, an increasing number of eutectogels fabricated through these methods have been reported in the literature. For example, de Lacalle *et al.* investigated the development of hydrophobic eutectogels for underwater electromyography (EMG) recording using DLP 3D printing, obtaining excellent printing resolution and demonstrating the fast and cost-effective manufacturing.[7] Another interesting optimization involved both the formulation and the printing parameters in order to obtain high-resolution microstructures in eutectogel-based electrodes.[8] It was demonstrated that different electrode patterns affect their performance in EMG recordings, further highlighting the benefits of 3D printing in the fabrication of eutectogels for bioelectronics applications.

In the last decade, there has been a megatrend in developing bio-based materials that can substitute oil-based ones. For this reason, the use of biomaterials from natural resources as the main components of eutectogels has increased, including polysaccharides, proteins and other biopolymers.[9–11] In order to obtain light-based 3D-printable eutectogels, these biopolymers are usually chemically modified, incorporating acrylate, methacrylate, and vinyl functionalities.[12,13] These functional-

[a]*Polymer Reaction Engineering Group, INTEC (Universidad Nacional del Litoral-CONICET), Güemes 3450, Santa Fe 3000, Argentina.*
E-mail: rjminari@santafe-conicet.gov.ar
[b]*Center for Cooperative Research in Biomaterials (CICBiomaGUNE), Basque Research and Technology Alliance (BRTA), Donostia-San Sebastián 20014, Spain*
[c]*Facultad de Ingeniería Química (Universidad Nacional del Litoral), Santiago del Estero 2829, Santa Fe 3000, Argentina*
[d]*POLYMAT and Department of Polymers and Advanced Materials: Physics, Chemistry and Technology, Faculty of Chemistry, University of the Basque Country UPV/EHU, Donostia-San Sebastián 20018, Spain*
[e]*POLYMAT, University of the Basque Country UPV/EHU, Joxe Mari Korta Center 72, Donostia-San Sebastian 20018, Spain. E-mail: david.mecerreyes@ehu.es*
[f]*Ikerbasque, Basque Foundation for Science, Plaza Euskadi 5, 48009 Bilbao, Spain*

ities participate in a radical polymerization process, resulting in the formation of a 3D crosslinked network. As an example, Locatelli *et al.* recently reported the development of fully bio-based photopolymerizable formulations based on acrylated epoxidized soybean oil and a natural DES for producing hydrophobic eutectogels *via* LCD 3D printing.[10] Interestingly, this work represents one of the first studies on bio-based 3D-printed eutectogels, a topic that remains largely unexplored.

On the other hand, there is a need to adapt eutectogels to emerging 3D printing technologies. For example, tomographic volumetric additive manufacturing (VAM) has emerged in the last years as a new technology in which the viscosity limitations typically encountered in VAT photopolymerization (VP) processes are absent.[14,15] To date, to the best of our knowledge, this technique has not been explored for eutectogel fabrication.

In this work, we report for the first time the development of photocurable eutectogel formulations based on casein, a milk-derived protein highly available at elevated purity. First, we investigated the chemical modification of casein with acrylic groups. Then, the incorporation of two different ionically conductive DESs was explored, enabling the fabrication of eutectogels *via* photopolymerization. Owing to their intrinsic ionic conductivity, these eutectogels were evaluated as sensitive pressure sensors. Finally, three-dimensional eutectogels were successfully fabricated using two different additive manufacturing techniques: DLP and VAM 3D printing technologies.

2. Materials and methods

2.1. Materials

Technical grade casein from bovine milk (Sigma-Aldrich), glycidyl methacrylate (GMA, 97%, Alfa Aesar), sodium carbonate (Na_2CO_3, Sigma-Aldrich), poly(ethylene glycol) diacrylate (PEGDA, M_n = 575 g mol^{-1}, Sigma-Aldrich), riboflavin (RF, Sigma-Aldrich) and triethanolamine (TEA, 98%, Sigma-Aldrich). Lithium phenyl-2,4,6-trimethylbenzoylphosphinate (LAP, ≥95% purity Sigma-Aldrich), glycerol (Cicarelli), sucrose (Anedra), betaine (≥98%, Sigma-Aldrich) and pyridine (Sigma-Aldrich) were used as received. Ultrapure water was employed throughout the work.

2.2. Synthesis of methacrylated casein

Methacrylated casein (M-casein) was synthesized *via* an amine-glycidyl ether reaction (Fig. S1A). Briefly, casein (25 g) was dissolved in an aqueous medium (208 g), adjusted to pH 10 using 0.4 wt% Na_2CO_3, and maintained at 50 °C. Upon complete dissolution of the protein, GMA (4.74 g) was introduced, and the reaction was allowed to proceed at 50 °C for 4 h under continuous stirring. The resulting solution was subsequently lyophilized to obtain dry M-casein and to remove any residual unreacted GMA.

2.3. Preparation of M-casein based photopolymerizable formulations

Two different DESs were prepared using betaine (Bet) as the HBA and two compounds as HBDs, namely glycerol (Gly) and sucrose (Suc). The resulting DESs were Bet : Gly (1 : 2 molar ratio) and Bet : Suc (1 : 1 molar ratio, 20% w/w water).[16] For DES preparation, the required amounts of each component were mixed and heated at 90 °C with continuous stirring until a homogeneous liquid was obtained.

In order to prepare the photopolymerizable formulations, first the RF photoinitiator was dissolved in ultrapure water at 70 °C. Next, the RF solution was cooled down to 50 °C, and M-casein and DES were added. Once the protein was completely dissolved, PEGDA was introduced, and the solution was kept at 50 °C with agitation for 10 minutes. TEA was added to the final solution when it was employed as a co-initiator. The final proportion of DES/water (hydrated DESs) in the eutectogel formulation was 50/50 wt%. Additional formulations without DES were prepared for preliminary photopolymerization studies. For the 3D printable formulations, the LAP photoinitiator was also used, instead of the RF/TEA system. LAP was first dissolved in a small volume of water and then added to the M-casein/hydrated DES solution under stirring until complete dissolution.

2.4. Bulk photopolymerization of M-casein based formulations

Photopolymerizable formulations were placed in a homemade closed chamber. This chamber consisted of a 1 mm thick silicone mold sealed with a fluorinated ethylene propylene (FEP) film to prevent water evaporation during photo-crosslinking. Subsequently, photopolymerization was conducted using a custom-made portable irradiator equipped with four LEDs (10 W, 365 nm) for 20 minutes (10 min on each side of the gel).

2.5. 3D printing of casein-based eutectogels

The models designed for printing were sent to the commercially available tomographic volumetric printer (Tomolite v2.0, Readily3D SA), using a light source centered at 400 nm. CAD files were transferred into the printer using the Apparite software. The energy density used for the 3D printing was 1200 mJ cm^{-3}.

DLP printed 3D objects were processed on a commercial Asiga Max-UV DLP 3D printer with a LED source centered at 385 nm. Computer-designed 3D objects were prepared for printing in the Asiga Composer software. To minimize the use of resin a home-built printing platform (aluminum, ∅ 3 cm) was used. The optimized printing parameters were 10 s burn-in layer, 7.5 s exposure time and 100 μm layer thickness at an intensity of 20 mW cm^{-2}.

2.6. NMR spectroscopy

The casein degree of methacrylation was quantified by ^{1}H NMR spectroscopy using a Bruker Avance II (300 MHz) instru-

ment. Spectra were acquired from dissolved lyophilized M-casein in deuterium oxide (D_2O) with pyridine as an internal standard. Pyridine presents three well-resolved signals at 7.35, 7.75, and 8.40 ppm, which do not overlap with the resonances of casein or GMA. The vinyl proton signals of incorporated methacrylic groups at 6.05 and 5.65 ppm were integrated and normalized against the integral of the pyridine signal at 8.40 ppm, selected as the reference peak. A calibration curve was established beforehand by correlating the integrated peak area ratios with known concentration ratios of GMA and pyridine.

2.7. Fourier transform infrared (FTIR) spectroscopy

Casein methacrylation was also confirmed by Attenuated Total Reflection (ATR)-FTIR spectroscopy in a NICOLET 8700 Thermo Scientific spectrometer, utilizing a universal ATR sampling accessory equipped with a ZnSe window. The spectra were obtained by averaging 50 scans within the 4000–650 cm^{-1} range, with a resolution of 4 cm^{-1}.

In addition, the photopolymerization kinetics of M-casein/PEGDA formulations were assessed by *in situ* near-infrared (NIR)-FTIR absorption spectroscopy, where the disappearance of the 6182 cm^{-1} absorption peaks, corresponding to the consumption of vinyl (C=C) groups, was monitored. Spectra were recorded using the NICOLET 8700 spectrophotometer. Liquid formulations were analyzed within a customized chamber, which consisted of a silicone spacer with an optical path length of 1 mm placed between two glass windows. For *in situ* excitation, the previously described portable irradiator (10 watts at 365 nm) was utilized. The irradiator was positioned inside the IR spectrometer to illuminate the sample during the experiment, and it was then promptly removed just before acquiring the spectra.

The fraction of polymerized vinyl groups (from M-casein and PEGDA) expressed as a percent of conversion was calculated from the area of the absorption peak at 6182 cm^{-1}, using eqn (1), where A_0 is the peak area before the photopolymerization and A_t the peak area at different photopolymerization times.

$$\text{Conversion}\,(\%) = 100 \times \frac{A_t - A_0}{A_0} \quad (1)$$

2.8. Insoluble fraction of crosslinked M-casein/PEGDA formulations

The insoluble fraction of M-casein/PEGDA formulations was determined as the portion that remains insoluble after being extracted with a suitable solvent, and it provides an indication of the degree of crosslinking.

To measure this, a specific amount of dried gel obtained through lyophilization was subjected to extraction with water at 37 °C for 24 hours to eliminate the non-crosslinked fraction. Subsequently, the extracted gel was dried at 60 °C until a constant weight was achieved. The insoluble fraction (%) was calculated using eqn (2), where W_i and W_f are the initial and final gel weights, respectively.

$$\text{Insoluble fraction}\,(\%) = 100 \times \left(\frac{W_f}{W_i}\right) \quad (2)$$

2.9. Eutectogel water content

Water content of eutectogels was gravimetrically evaluated. Circular samples (8 mm in diameter) were weighed immediately after polymerization and then maintained in a controlled atmosphere of 25 °C and 75% relative humidity (RH) until reaching a constant weight. The equilibrium water content (%) of eutectogels at 25 °C and 75% RH was determined by using the following equation,

$$\text{Water content}\,(\%) = 100 \times \left(1 - \frac{W_0 - W_1}{W_0^{\text{water}}}\right) \quad (3)$$

where W_0 and W_1 are the initial and final gel weights, respectively, and W_0^{water} represented the initial weight of water in the eutectogel, calculated from the formulation and the W_0. Due to the fact that the water content of the eutectogel could depend on the environmental conditions, eutectogels were exposed to the controlled humidity and temperature atmosphere (75% RH at 25 °C) during 24 h prior to the other characterizations described below.

2.10. UV-Vis transmittance measurements

UV-Vis transmittance measurements were performed to assess the optical transparency of the precursor polymerization solutions. Spectra were obtained using a Jasco V-730 UV-Vis spectrophotometer, and the transmittance at 600 nm was selected for comparison among formulations. Measurements were carried out in 10 mm path-length cuvettes using deionized water as the blank.

2.11. Thermogravimetric characterization

Thermogravimetric analysis (TGA) was performed using a (TGA Q500 of TA instruments). Around 7 mg of sample was placed in the sample holder and heated from 30 to 500 °C at a heating rate of 10 °C min^{-1} under a nitrogen atmosphere. The weight loss as a function of temperature was recorded to assess the thermal stability of the eutectogels.

2.12. Electrochemical impedance spectroscopy (EIS)

Electrochemical impedance spectroscopy (EIS) measurements were performed using a PalmSens potentiostat–galvanostat. Circular samples (8 mm in diameter) were mounted in a two-electrode cell. Prior to each measurement, the system was equilibrated at the target temperature (25 °C) for 20 minutes to ensure thermal stability. The frequency sweep spanned from 10^5 Hz to 1 Hz, with an applied voltage amplitude of 10 mV. AC voltage amplitudes between 5 and 20 mV were tested to ensure operation within the linear response regime, and an amplitude of 10 mV was selected. The Nyquist plot was obtained by plotting the imaginary against the real part of the impedance at each frequency. The Randles circuit was used as the equivalent circuit, and the experimental data were fitted to obtain the different circuit elements using PSTrace software.

The ionic conductivity (σ) was determined by the following equation:

$$\sigma = \frac{l}{R_{gel}S} \quad (4)$$

where l is the gel thickness, S the contact area between the sample and the electrode, and R_{gel} the resistance obtained from the Nyquist plot. All measurements were performed in triplicate.

2.13. (Photo)rheology

Viscosity measurements of photopolymerizable liquid formulations were performed using an MCR302 Anton Paar rheometer. The formulations were placed on a 25 mm diameter parallel plate with a 0.1 mm gap, and the viscosity was recorded over a shear rate range of 0.1–1000 s^{-1} at 25 °C.

In addition, photo-rheometry experiments were conducted in the same rheometer equipped with an OmniCure Series 1500 UV source (wavelength = 365 nm, light intensity = 17.75 mW cm^{-2}). The photopolymerizable liquid formulations were placed on a 25 mm diameter parallel plate with a 0.1 mm gap and the evolution of the dynamic (storage and loss) moduli were monitored over time at a frequency of 1 Hz, 0.1% of strain, and 23 °C. The UV light was turned on 50 s after the start of the measurement.

Moreover, rheological studies on circular samples of eutectogels (approximate thickness of 1 mm) were conducted using a HAAKE MARS 40 rheometer, employing a 35 mm parallel plate geometry. The measurement was conducted using a frequency sweep from 0.1 to 10 Hz, with an applied strain of 0.5% at 25 °C.

2.14. Compression test

Loading–unloading compression tests of the eutectogels were performed using an INSTRON 3344 universal testing machine at 25 °C. Circular specimens with a diameter of 8 mm and a thickness of 2 mm were compressed with a 10 mm flat-ended probe at a constant rate of 1 mm min^{-1} until the samples reached 35% strain (relative to their original thickness), followed by unloading at the same rate. Four specimens per sample were tested.

Different parameters were obtained from the compressive curves: the compressive modulus was calculated as the slope in the low-strain linear region; the residual deformation was determined as the strain at which the stress returns to zero during unloading; the hysteresis area was calculated as the area between the loading and unloading curves; and finally, the stress at 35% strain was also determined from the curves.

2.15. Pressure sensor test

As proof of concept and with the aim of evaluating the sensor capabilities of the eutectogels, a pressure sensor was constructed. For this purpose, a disc of eutectogel was attached to copper electrodes in both planar faces and connected to a multimeter. The pressure sensitivity (S) was determined from the slope of a $\Delta R/R_0$ *vs.* pressure curve obtained by compressing the eutectogel at 0.5 mm min^{-1} using the universal testing machine previously described. Moreover, the resistance was recorded during the sequential application of different calibrated loads of 30 g and 50 g.

3. Results and discussion

3.1. Preparation of bio-based casein eutectogels

With the aim of preparing a bio-based eutectogel with a chemically crosslinked matrix, in a first step M-casein was synthesized. M-casein synthesis involves the ring opening of the epoxide group of GMA, with the ε-NH_2 of lysine acting as a nucleophile, generating an amine group with a methacrylic moiety (Fig. S1A). The success of the casein modification was confirmed by ATR-FTIR (Fig. S1B), where new bands can be detected at 1715 and 1165 cm^{-1} associated with the stretching vibration of C═O and the asymmetric stretch of C–O–C, respectively, from the attached methacrylic group. Furthermore, ^{1}H NMR (Fig. S2) also confirmed the appearance of the methacrylic characteristic protons of methacrylic groups from GMA in M-casein. The resulting incorporated methacrylic groups were determined to be 26.7 mol of GMA per mol of casein, representing a reaction efficiency of 67%, based on the 40 mol of GMA per mol casein used in the methacrylation reaction.

Next, a preliminary screening was conducted to evaluate the photopolymerization ability of M-casein/PEGDA formulations, with the aim of determining the concentrations of both components required to obtain a gel-like structure. In addition, the use of riboflavin (RF) (5×10^{-4} M) as a photoinitiator was initially explored. RF is a type II photoinitiator, forming a dual component photoinitiation system with an electron donor serving as a co-initiator. However, the photo-crosslinking of proteins using RF without an additional co-initiator has been reported, because tyrosine residues participate in the photoinitiation reaction, leading to the formation of tyrosyl radicals.[17,18]

This first screening was performed with aqueous formulations (*i.e.*, without DES) varying the concentration of M-casein and PEGDA. M-casein concentrations ranging from 15 to 25 wt% relative to water content were analyzed, gradually increasing the PEGDA content (from 0 to 35%, relative to M-casein). Fig. S3 shows the values of insoluble fraction determined for each photocrosslinked formulation, which are indicative of the extent of polymerization (insoluble fraction obtained from the dried crosslinked sample after extraction with water). The formulations that did not result in a gel-like structure are indicated in red. In these cases, radical polymerization occurred as evidenced by the increase in the viscosity of the reaction medium, but the total concentration of reactive molecules (M-casein and PEGDA) was not enough to form a gel.

Using 25 wt% M-casein, it is possible to obtain a gel without adding PEGDA and with a high insoluble fraction (86.4%). However, the formulations with lower concentration of M-casein can form a well-crosslinked network upon the

addition of PEGDA as a secondary crosslinker, with the required PEGDA concentration increasing as the M-casein content decreases. For example, a formulation with 15 wt% M-casein needs at least 30 wt% PEGDA to form a gel, with an insoluble fraction of 67.5%.

The photo-crosslinking of native proteins (*i.e.*, without polymerizable vinyl functionality) using RF as photoinitiator has been reported, since two tyrosyl radicals are able to form a dityrosine crosslink.[19] When 25 wt% of native casein was photopolymerized with RF, only an insoluble fraction of 2.3% was determined and no gel formation was observed, indicating that tyrosine-mediated crosslinking makes only a minor contribution to network formation compared with crosslinking through the methacrylic moieties of M-casein.

In addition to the photoinitiator system composed of RF, the system RF/TEA was analyzed, with TEA acting as a co-initiator.[20] Fig. S3B compares the photopolymerization kinetics with both initiator systems, which was determined following the consumption of C=C groups (corresponding to M-casein and PEGDA) by NIR-FTIR spectroscopy.[21,22] The photoinitiator composed solely of RF produced a slow polymerization with a lengthy inhibition period, even considering that the concentration of RF used here was significantly high (5×10^{-4} M), and was at the limit of its water solubility. The low efficiency of RF in the formation of free radicals could be associated with the low efficiency of tyrosine residues of casein in the photoinitiation reaction. Although the concentration of tyrosine residues was relatively high in the formulation (5×10^{-2} M, calculated considering a tyrosine concentration of 5.3 g per 100 g of casein), its efficiency in the photoinitiation reaction would be reduced by diffusive effects due to the high molecular weight of casein.[23] That is why the use of low molecular weight TEA (1×10^{-2} M) as a co-initiator generates a more efficient photoinitiation system that significantly increases the polymerization rate, even when using lower concentrations of RF (1×10^{-4} M).

For the eutectogel formation by photopolymerization, a mixed solution of water and DES, defined as hydrated DES, was used in a 1 : 1 weight ratio to make M-casein soluble (the protein is not soluble in pure DESs or in a hydrated DES with lower water contents). Considering the content of M-casein and PEGDA required to form a stable crosslinked structure (Fig. S3A), eutectogel formulations were prepared by dissolving 17.5 wt% of M-casein relative to the hydrated DES (which is the solubility limit of M-casein in this solution) and three different concentrations of PEGDA (30, 50 and 100 wt% relative to M-casein). The photoinitiation system was composed of RF (1×10^{-4} M) and TEA as a co-initiator (1×10^{-2} M). Fig. 1A illustrates the preparation method. The eutectogels were coded according to the PEGDA content and the DES used. Specifically, "P(X)" indicates the PEGDA content where X represents the concentration relative to the M-casein, while "D_1" and "D_2" refer to Bet/Gly and Bet/Suc DESs, respectively. For example: P(30)-D_1 refers to the eutectogel composed of 30% of PEGDA using Bet/Gly as the DES.

After photopolymerization, translucent eutectogels were obtained for formulation with low PEGDA content (30%), whereas those with high PEGDA content (100%) were opaque (Fig. 1B). Although the gels are of different sizes, because they are produced with molds of different diameters, no reduction in gel size was observed after photopolymerization. Gel opacity at high PEGDA concentration could be a consequence of the formation of PEGDA aggregates and/or casein micelles formation in the solution prior to curing, leading to increased light scattering and reduced transparency. To investigate this behavior, the transmittance at 600 nm of precursor solutions containing different PEGDA concentrations in the polymerization medium (water/D_1), in the absence and presence of M-casein, was evaluated (Fig. S4). In the absence of M-casein, the transmittance progressively decreased with increasing PEGDA content, which may be attributed to the formation of self-assembled PEGDA structures. In addition, precursor solutions containing M-casein in the absence of PEGDA already exhibited low transmittance values, suggesting the presence of casein micelles. These results support the hypothesis that both PEGDA aggregation and casein micelles contribute to the opacity observed in the corresponding eutectogels.

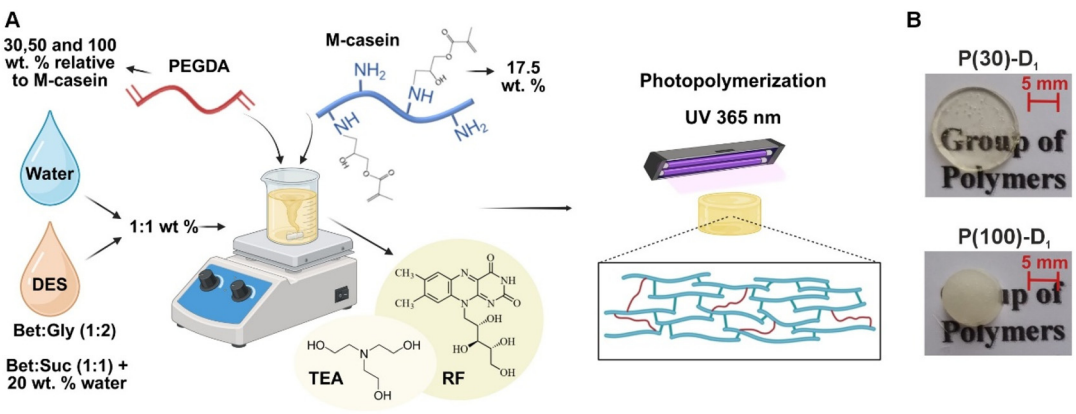

Fig. 1 (A) Preparation method for the M-casein eutectogels. (B) Images of two different eutectogels with different PEGDA content.

Due to the fact that water is incorporated in the formulation, the equilibrium water content in the eutectogels was evaluated, since their main properties, such as ionic conductivity and the mechanical performance, can be affected by this variable.[24] The gels were equilibrated under controlled humidity and temperature conditions (75% RH at 25 °C), and their weight was monitored after 24 and 48 h. No significant variation in water content was observed between these time intervals, indicating that equilibrium was reached within the first 24 h (Fig. S5 of the SI). Fig. 2A and B show the water content in the eutectogels containing D_1 and D_2, respectively, after exposure to a controlled environment (75% RH at 25 °C) during 24 h. Additionally, Table S1 in SI presents the equilibrium concentration of each component in the gels compared with the initial formulation (*i.e.* immediately after synthesis) The results indicate that all synthesized eutectogels lost a fraction of their initial weight of water. However, the equilibrium content of water in eutectogels with Bet/Suc DES was significantly lower (between 8 and 22 wt% relative to the DES content) than that of the eutectogels with Bet/Gly DES (between 73 and 78 wt%). This behavior can be attributed to the higher affinity of the Bet/Gly DES for water compared to Bet/Suc, resulting from stronger polar interactions between water molecules and glycerol than with sucrose.[16,25] To further characterize the water content in the gels, TGA was performed in two gel formulations, P(100)-D_1 and P(100)-D_2 (Fig. S6 of SI). In the case of P(100)-D_1, a 23.4% of weight loss was detected around 100 °C related to water evaporation, and for P(100)-D_2 the weight loss in this range of temperature was 6%. These results agree with the equilibrium water content determined gravimetrically (Table S1). Taking these results into account, eutectogels were exposed to a controlled environment (75% RH and 25 °C) during 24 h before characterizations, in order to analyze the eutectogel properties without variation in their content of water.

One of the parameters to be evaluated is photopolymerization kinetics. Therefore, M-casein/PEGDA systems in both D_1 and D_2 hydrated DES were analyzed by photorheology. Fig. 2C depicts the evolution of the storage shear modulus (G') and the loss shear modulus (G'') over time for the formulations P(50)-D_1 and P(50)-D_2, with UV irradiation initiated 50 s after the start of the measurement. The results show a slow increase in G' in both formulations after UV irradiation, which stabilizes after around 1600 s, achieving G' values of 6.6 and 65 kPa for P(50)-D_1 and P(50)-D_2, respectively. These results are consistent with the photopolymerization kinetics determined by NIR-FTIR with the RF/TEA photoinitiator system (Fig. S3B). Additionally, the higher values of G' compared to G'' indicate gel-like behavior, resulting from the formation of the cross-linked structure as the reaction proceeds. Interestingly, gel-like behavior is observed for both formulations before UV irradiation; however, it is more pronounced in the P(50)-D_2 one, probably arising from existing hydrogen bonds between sucrose and casein molecules. To test this hypothesis, the

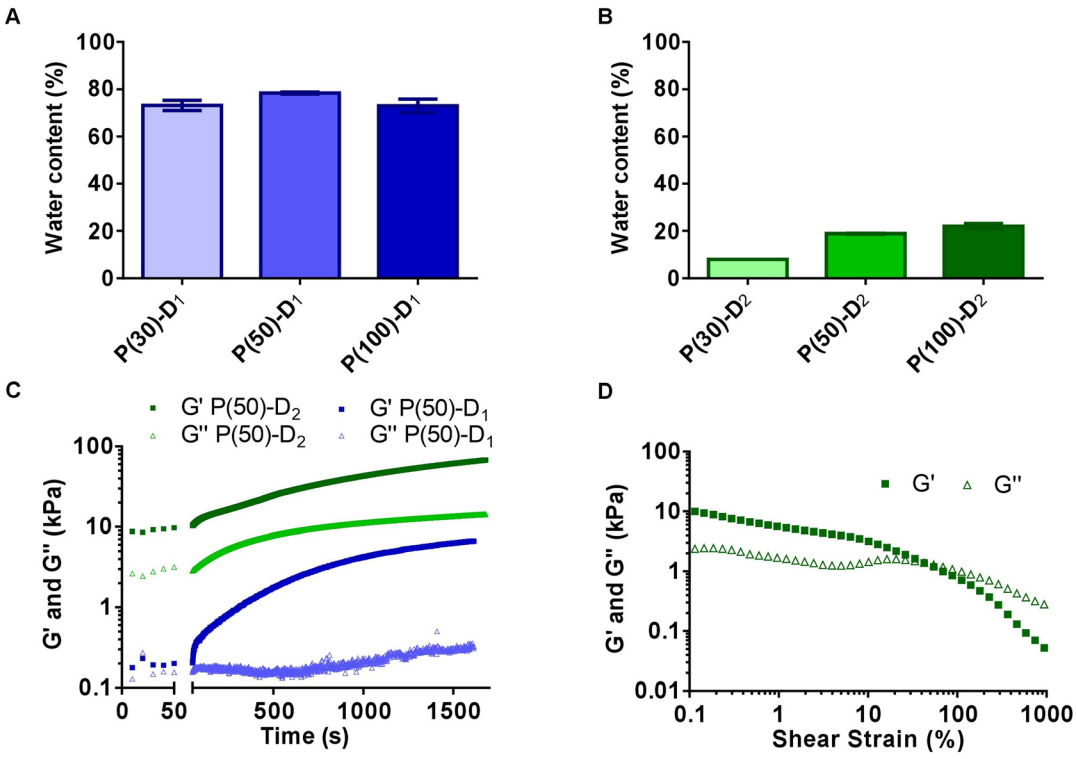

Fig. 2 Graph of equilibrium water content (wt% relative to the initial water content, eqn (3)) at 25 °C and 75% RH for each formulation: D_1 (A) and D_2 (B) based eutectogels. (C) Photorheology measurements comparing formulations with both DES types (D_1 in blue and D_2 in green) and 50% PEGDA content. (D) Shear strain sweep for P(50)-D_2 before photopolymerization.

shear strain sweep (Fig. 2D) on the uncured P(50)-D_2 formulation was performed, which showed the typical behavior of a supramolecular gel, with a pronounced decrease in G' due to the progressive breaking of reversible interactions, and a crossover of the moduli occurring at a strain of around 40%.[26,27]

3.2. Characterization of bio-based eutectogels based on casein

Eutectogels, defined as soft materials, possess viscoelastic properties which are commonly analyzed using rheological measurements.[28] For this reason, and with the aim of determining the viscoelastic behavior of the studied eutectogels, G' and G'' were obtained through a frequency sweep during a rheological test. All the formulations exhibited predominant elastic behavior with stable G' values higher than G'' throughout the entire frequency range studied, indicating a structurally stable crosslinked network (Fig. S7). Additionally, eutectogels with higher PEGDA content show superior G' values, with a difference of around 6 kPa between 100% and 30% of PEGDA in D_1-based eutectogels, and around 40 kPa between these two PEGDA contents in D_2-based eutectogels. This is a consequence of a more highly interconnected network, which increases their strength.[29] It is also worth noting that a similar trend is observed between the eutectogels with different DESs, where the eutectogels with D_2 present a higher G' than those with D_1 (around 40 kPa between formulations with 100% PEGDA) (Fig. 3A). Two reasons could explain this difference. On one hand, the additional physical interactions in eutectogels containing D_2 may enhance their elastic behavior. On the other hand, this effect is most likely attributed to the lower water content in these eutectogels, which increases the solid content and, consequently, their elastic response.

The increased crosslinking density in eutectogels with greater PEGDA content is also evident in their mechanical response during loading–unloading compression tests. Fig. 3B and C show the stress–strain curves for eutectogels with different PEGDA content and DES type. As expected, the compression modulus (Fig. 3D) and stress at 35% of strain (Fig. 3E) increase with PEGDA content, with a more notable difference between the samples containing 100% of PEGDA and those with 30 or 50% of PEGDA. Consistent with the rheological study, eutectogels with D_2 exhibit higher values of these parameters than those with D_1. The stress at 35% of strain for the 100% PEGDA formulation has values of 47 kPa for D_1 and 166 kPa for D_2, whereas the lower values for 30% PEGDA formulations are around 7.4 kPa for D_1 and 56 kPa for D_2. The compression moduli, ranging from 150 to 253 kPa for eutectogels with D_2 and from 17 to 92 kPa for D_1, are consistent with those reported for soft materials employed in bioelectronic applications, where low modulus is adequate for biomechanical interact with biological tissue (within the tens to hundreds of kPa range).[30–32] Furthermore, the loading–unloading curves are also useful for studying viscoelastic properties through the appearance of a hysteresis phenomenon which is observed when the loading and unloading stress–strain curves do not match, indicating an energy dissipation characteristic of viscoelastic behavior. The hysteresis area and residual deformation are parameters commonly used to quantify the viscoelasticity of a material: values close to zero indicate purely elastic behavior, whereas higher values reflect a departure from ideal elasticity.[33,34] In line with the previous compression parameters, eutectogels containing D_2 and higher PEGDA content exhibit greater elasticity, as evidenced by lower hysteresis area (Fig. 3F) and reduced residual deformation (Fig. 3G). Additionally, eutectogels show stable mechanical properties, as consecutive stress–strain curves exhibit minimal changes (*i.e.* approximately the same hysteresis area and maximum compressive stress) and nearly overlap after 5 loading–unloading cycles (Fig. S8). This behavior indicates that the gel microstructure was not significantly altered under the repeated compression cycles.

One of the most interesting properties of these eutectogels is the ionic conductivity, due to the incorporation of ionic DES. This parameter was determined from impedance measurements over a range of applied voltage frequencies during EIS tests at room temperature. Fig. 4A depicts the obtained Nyquist plots, which exhibit a semicircle in the high-frequency region associated with kinetics phenomena, and a straight line in the low-frequency region related to mass transfer processes. These plots display the characteristic shape of a Randles circuit (Fig. 4B), which is commonly used to fit EIS spectra of gel electrolytes in contact with electrodes.[7,35] The corresponding theoretical Nyquist plots for the Randles circuit in the high-frequency region are also shown in Fig. 4A as continuous lines. The values of each circuit element were obtained (Fig. S9), and the ionic conductivity of eutectogels was calculated from the fitted R_u values. Fig. 4C and D show the ionic conductivity of each formulation with values around 1×10^{-3} S cm^{-1} for D_1-based eutectogels and 6×10^{-5} S cm^{-1} for D_2-based ones. The difference in ionic conductivity between these systems is mainly attributed to their different water contents. A higher water content promotes ionic species mobility, and hence the eutectogels containing D_1 present higher conductivity than those containing D_2, whose water content is considerably lower (Table S1 of SI).[24] This trend is also observed in D_1-based gels with different PEGDA content, where the slight difference in ionic conductivity observed appears to be primarily related to the water : DES weight ratio. P(50)-D_1 exhibited the highest ionic conductivity, corresponding to the highest water : DES ratio (0.78 : 1), whereas P(30)-D_1 and P(100)-D_1 presented lower ionic conductivity and water content (ratios 0.73 : 1). No significant differences were observed when varying the PEGDA content in both D_1 and D_2-based gels. In either case, the ionic conductivity is suggested to be governed by the percolated liquid rather than by the crosslink level of the matrix, which could also affect the ion mobility within the eutectogel. D_1-based formulations exhibit conductivity values comparable to those of other eutectogels used for bioelectronics applications.[36–38]

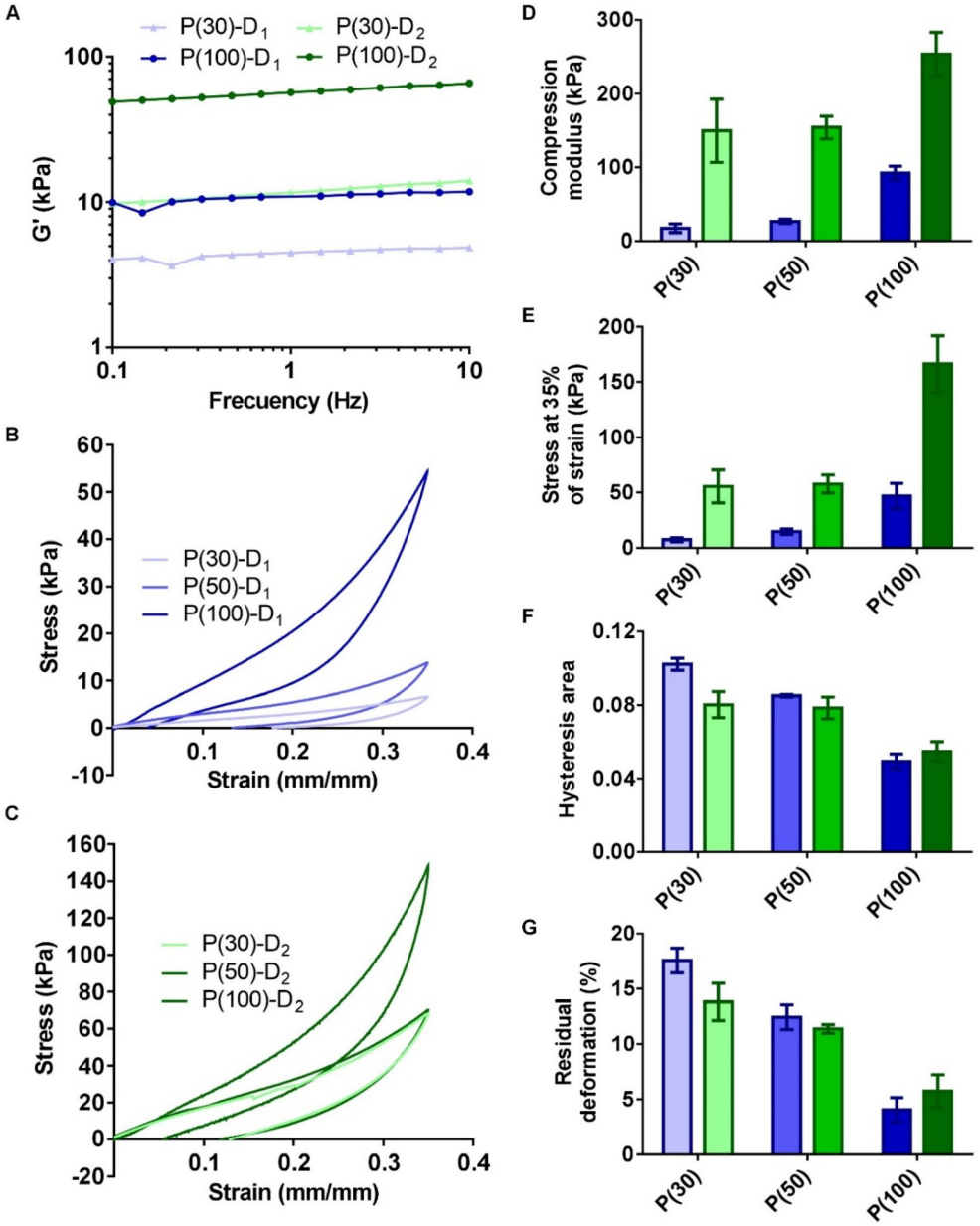

Fig. 3 (A) *G′* as a function of frequency. Loading–unloading compression test of D_1-based formulation (B) and D_2-based formulation (C), and mechanical properties such as (D) compression modulus, (E) stress at 35% strain, (F) hysteresis area, and (G) residual deformation for eutectogels with different DES and PEGDA content.

3.3. Application of bio-based eutectogels in pressure sensors

As proof of concept, a pressure sensor based on the P(100)-D_1 formulation was fabricated and its performance was evaluated. This gel was selected due to its high ionic conductivity and good mechanical properties. The electrical resistance (R) was registered during a compressive test, and the relative resistance variation ($\Delta R/R_0$) was calculated and plotted as a function of the applied pressure (Fig. 5A). From this relationship, the pressure sensitivity (S) was determined, obtaining a value of 0.7 kPa^{-1}, which is consistent with previously reported values for eutectogels.[39,40] For example, Ma *et al.* developed a pressure sensor based on a dual network eutectogel composed of a prepolymerized network of [2-(methacryloyloxy)ethyl]dimethyl-(3-sulfopropyl) (DMAPS) and physically crosslinked acrylic acid-*N*-(2-hydroxyethyl)acrylamide copolymers (p(AA-*co*-HEMAA)), with a S value of 0.684 kPa^{-1} over a pressure range of 0–14 kPa.[40] On the other hand, Fig. 5B shows the evolution of the resistance (R) over successive compression-release cycles, using 30 and 50 g loads, highlighting the reproducibility of the sensor response. A

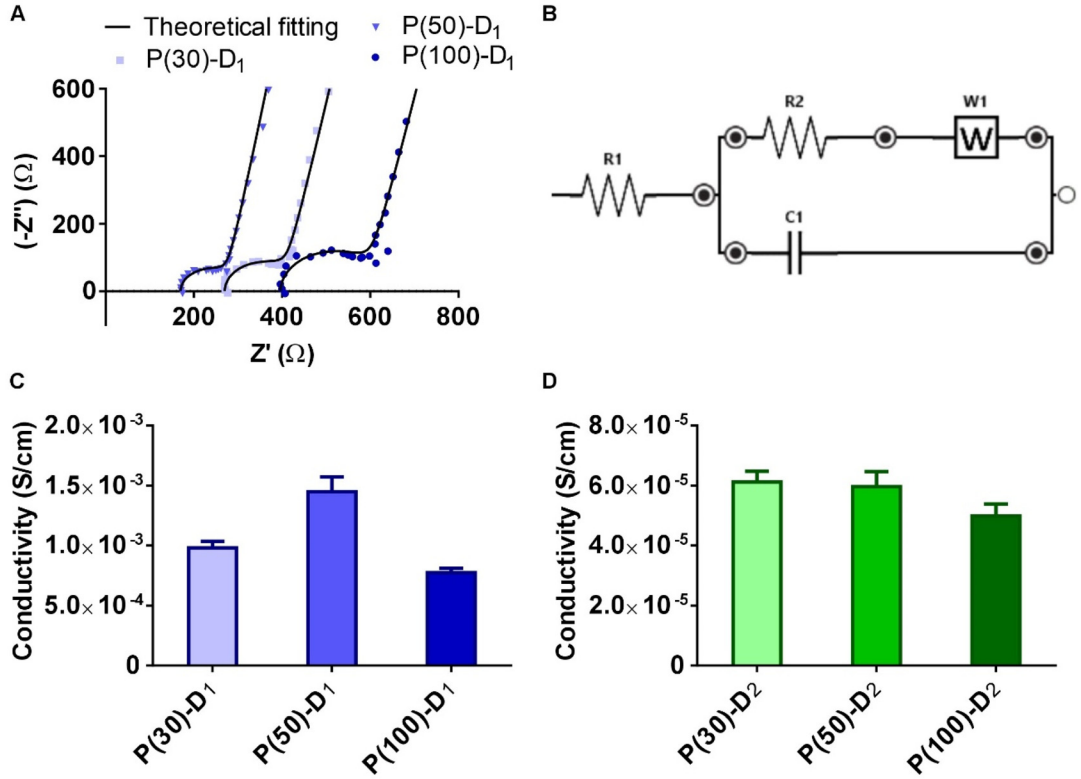

Fig. 4 (A) Nyquist plot for D1-based eutectogels with different PEGDA content and the theoretical fitting (black line). (B) Randles circuit with the different elements: R: resistor, C: capacitor and W: Warburg element. Ionic conductivity for eutectogels (C) D_1-based formulation and (D) D_2-based formulation.

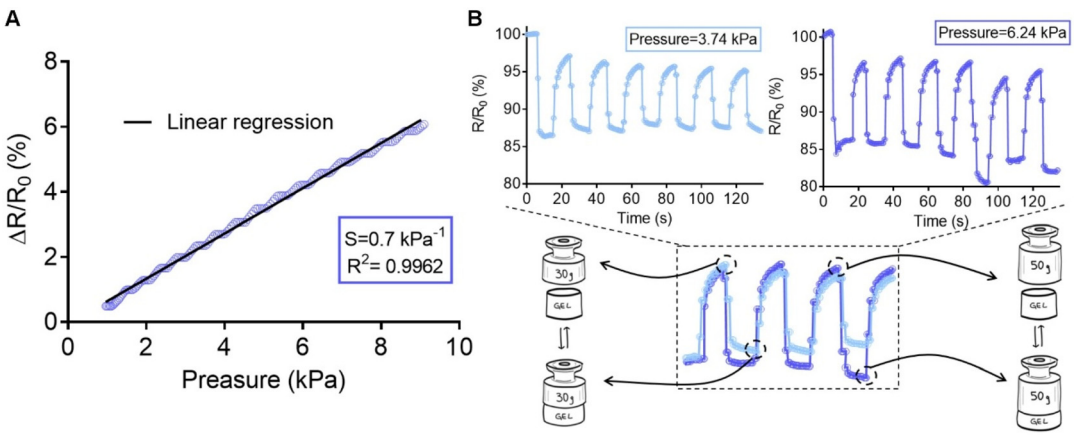

Fig. 5 (A) Relative resistance as a function of pressure, along with linear regression used for calculating sensitivity. (B) Successive compression-release cycles showing the resistance over time under applied loads of 30 g (left) and 50 g (right), together with a comparison of both signals (below).

clear difference between both conditions is observed, with higher signal amplitudes obtained under the 50 g load.

3.4. Processability of bio-based casein eutectogels by 3D printing

The photopolymerizable nature of this system makes it suitable for fabricating eutectogels with different predesigned forms by light-based 3D printing technologies. Two different 3D printing techniques were explored with M-casein based formulations, tomographic VAM and DLP 3D printing. Particularly, VAM is a new technology with different benefits compared to the traditional VP technologies, like rapid printing, smooth finish without layers and the possibility of printing without support.[14]

The designed formulation containing 17.5 wt% M-casein, D_1 and the RF/TEA photoinitiator system was initially evaluated for printing with both technologies. D_1 formulation was chosen for 3D printing due to the high conductivity values and also because it is the formulation which loses less water, allowing to obtain a final piece that maintains its shape after 3D printing. However, several limitations were identified. During DLP printing, significantly long curing times (180 s) were required to form a cured layer. In addition, the high viscosity of the formulation promoted the detachment of the cured layers from the build platform, preventing successful printing. On the other hand, for VAM, formulation transparency is a key parameter for obtaining parts with good resolution. However, the formulation containing 17.5% of M-casein exhibited reduced transparency, as these molecules form micelles that scatter light. This, combined with the slow reaction kinetics of the RF/TEA system, was insufficient for a 3D printing process, even under high light intensity conditions (50 mW cm^{-2} for 300 s). In this context, modifications to the M-casein based formulation were necessary to enable successful printing.

First, the reduction of the M-casein concentration was considered to decrease the formulation viscosity and improve transparency. Reducing viscosity can promote the interaction of reactive functionalities, leading to faster cure rates and shorter construction times. Fig. 6A compares the viscosity of formulations containing 17.5 wt% and 12.5 wt% M-casein (with D_1), showing that reducing the M-casein content to 12.5 wt% resulted in a viscosity below 10 000 cP, which is more suitable for DLP 3D printing.[41,42] Moreover, this lower M-casein concentration formulation exhibited improved transparency.

On the other hand, the use of an alternative photoinitiation system was considered. Lithium phenyl-2,4,6-trimethylbenzoylphosphinate (LAP), a commonly used photoinitiator, was selected due to its fast kinetics and biocompatibility.[43,44] Photorheology confirmed faster photopolymerization kinetics for the 12.5 wt% M-casein formulation containing 0.1 wt% relative to M-casein of LAP (Fig. 6B), compared to the original formulation with 17.5 wt% of M-casein with the RF/TEA photoinitiation system (Fig. 6C). Furthermore, for formulations with LAP, both containing 12.5 and 17.5 wt% of M-casein, the time required to reach complete polymerization was similar, while G' was higher at a M-casein concentration of 17.5 wt%, due to the formation of a highly crosslinked network (Fig. S10 in SI). Whereas the formulation containing LAP reached the G' plateau 30 s after irradiation was initiated, the RF/TEA formulation did not reach this condition even after 1500 s, indicating slower reaction kinetics compared to other liquid resin formulations. These results support the use of this photoinitiator system for VP, where relatively short curing times are sufficient to form self-supporting gel layers during typical printing processes.[35]

In order to evaluate the printability of this modified formulation (M-casein 12.5 wt%, P(30)-D_1-12.5), DLP 3D printing was employed to fabricate eutectogels. A 3D model containing pyramids of different sizes was employed, with heights and diameters ranging from 1 mm to 5 mm, to assess the resolution of the printed structures. Fig. 6D shows the 3D-printed eutectogel alongside the corresponding 3D model for comparison. As observed, the larger pyramids (1.5–5 mm) were successfully printed, exhibiting well-defined shapes and surface finishes. However, the smallest pyramid (1 mm) could not be fully resolved, indicating the resolution limit of this formulation.

In addition, using a similar formulation (P(40)-D_1-12.5) the 3D printing parameters for the tomographic volumetric 3D printing were optimized by irradiating the formation of eutectogel in different dot regions using exposure times from 50 to 300 s and light intensities between 17.32 and 50 mW cm^{-2} (Fig. 6E). After this optimization, an energy density of 1200 mJ cm^{-3} was determined and employed for printing. Fig. 6F shows a chess pawn shaped eutectogel obtained by VAM. Compared with the CAD model, the overall geometry and general shape of the chess pawn was reproduced, but with a suboptimal resolution, as evidenced by the low definition of finer features. This might be related to the absence of the total optical transparency of the formulation required in this technology, which can deeply affect accurate and high-resolution printing. Despite these limitations, these results demonstrate the feasibility of processing this type of formulation by volumetric 3D printing and highlight the potential for further improvements through formulation optimization. We observed that VAM and DLP printing approaches exhibit complementary advantages. VAM enables the fabrication of designs with a reduced working volume, resulting in lower overall resin consumption for similar geometry. In contrast, DLP processing of comparable formulations provides significantly higher resolution and improved feature definition, while maintaining processing times comparable to those achieved with VAM. To the best of our knowledge, this represents the first report of eutectogel printing using this technology.

The formulations evaluated for 3D printing with 12.5 wt% of M-casein (P(30)-D_1-12.5 and P(40)-D_1-12.5) were further characterized by EIS and compression tests.

The ionic conductivity of P(30)-D_1-12.5 and P(40)-D_1-12.5 gels were 1.80×10^{-2} and 1.17×10^{-2} S cm^{-1}, respectively (Table S2). Furthermore, higher ionic conductivity was observed in these gels containing 12.5 wt% M-casein compared to the 17.5 wt% M-casein formulations (Fig. 4C). This behavior may be attributed to a lower crosslinking density, resulting in enhanced ionic mobility and, consequently, increased ionic conductivity.

Regarding mechanical properties, P(30)-D_1-12.5 and P(40)-D_1-12.5 formulations show no significant changes during repeated loading and unloading compression cycles, indicating also good mechanical stability (Fig. S11A and B). Furthermore, Fig. S11C to F shows the different mechanical properties calculated for each formulation. Overall, P(40)-D_1-12.5 shows higher compression modulus and stress at 35% of strain than the P(30)-D_1-12.5 formulation, attributed to the higher PEGDA content. The difference observed in hysteresis area and residual deformation is negligible. Additionally, when comparing the P(30)-D_1 formulations containing 17.5

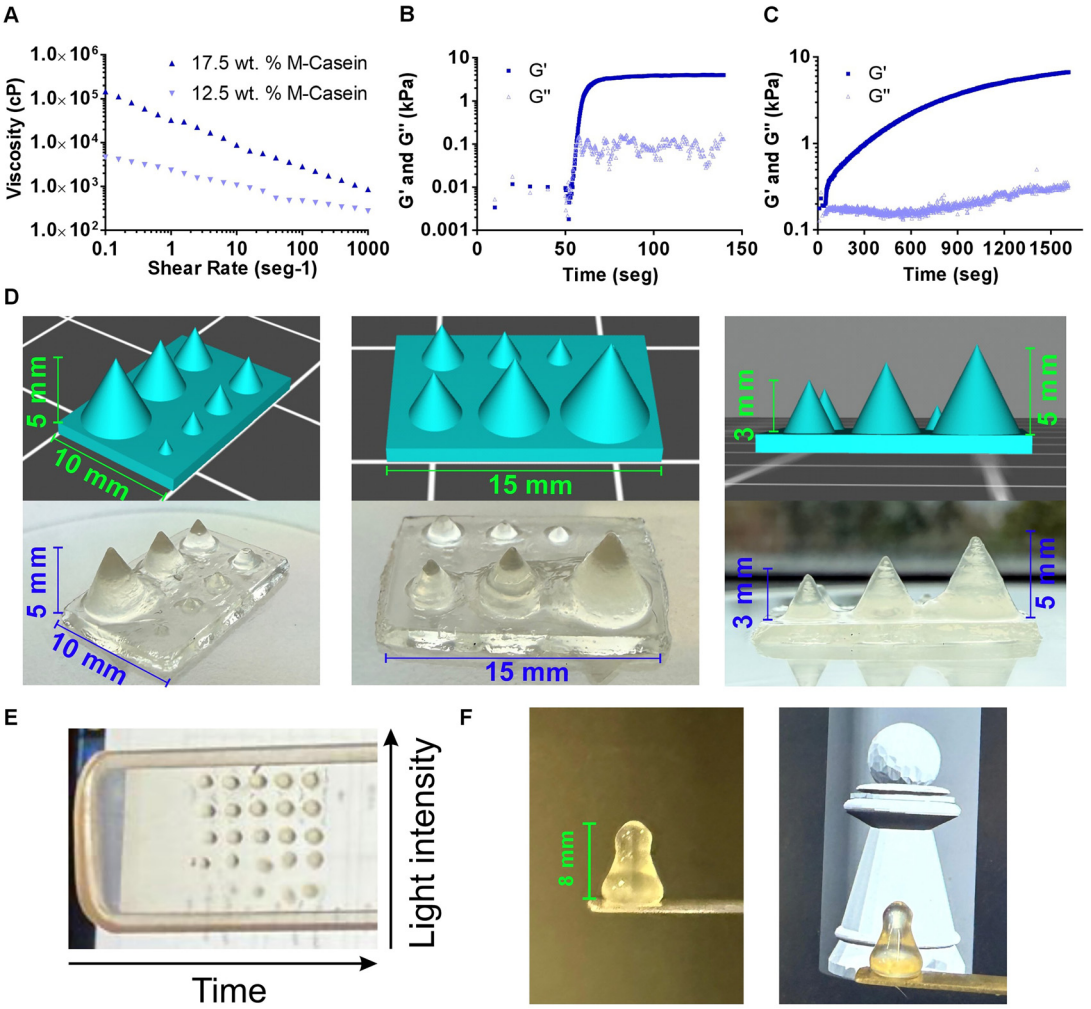

Fig. 6 (A) Viscosity evolution through a range of shear rates of different formulations with different M-casein content (12.5 and 17.5 wt%). Photorheology comparing the use of LAP as photoinitiator in formulation containing 12.5 wt% of M-casein (P(30)-D_1-12.5), (B) and RF/TEA photoinitiation system in formulation containing 17.5 wt% of M-casein (P(50)-D_1) (C). (D) Images of the 3D eutectogel pieces (P(30)-D_1-12.5) printed using the DLP vat 3D printer and their corresponding 3D models. (E) Picture of the gel dots obtained in the parameter optimization for the volumetric 3D printing using P(40)-D_1-12.5 formulation. (F) Images of the 3D eutectogel pieces (P(40)-D_1-12.5) printed using the volumetric 3D printer and the corresponding 3D models.

and 12.5 wt% M-casein, the first exhibited a higher compression modulus (17 kPa) than the latter (10 kPa), which can be attributed to its higher solid content.

4. Conclusion

In this work, eutectogels based on the protein casein were prepared. For that, M-casein was synthesized to incorporate methacrylic functional groups in the protein structure, therefore being capable of crosslinking during photopolymerization, while PEGDA acted as an additional crosslinker. The eutectogel formulation also included two DESs and a photoinitiation system composed of RF and TEA. By varying the PEGDA content and DES type, eutectogels with different crosslinking degrees and water contents were obtained, resulting in a library of eutectogel materials with tunable properties.

The viscoelastic properties of the eutectogels showed a predominant elastic behavior with compression moduli ranging from 17 to 253 kPa, stress at 35% of strain from 7.4 to 166 kPa, with a clear trend toward higher values in formulations with Bet/Suc DES and high PEGDA contents. This was attributed to the higher crosslinked matrix in eutectogels with more PEGDA and to the lower water content in Bet/Suc-based formulations, leading in a superior solid fraction.

The water content also affected the ionic conductivity with a clear difference between Bet/Suc-based formulations (around 6×10^{-5} S cm^{-1}) compared to Bet/Gly-based formulations (around 1×10^{-3} S cm^{-1}), where the latter exhibited higher conductivity due to their superior moisture content, which promotes ion transport. Based on the long-term elasticity and

the ionic conductivity of casein based eutectogels, their potential for bioelectronics was evaluated by assembling a pressure sensor, which exhibited a sensitivity of 0.7 kPa^{-1} and stable responses under repeated loading cycles.

Finally, the formulations were adapted for the requirements of tomographic volumetric and DLP 3D printing, enabling the fabrication of eutectogels with predesigned architecture. Overall, these results demonstrate that the developed bio-based eutectogels combine tunable mechanical properties, ionic conductivity, and printability, making them promising candidates for sustainable soft bioelectronics applications.

Conflicts of interest

There are no conflicts to declare.

Data availability

All data supporting the findings of this study are included in the article and its supplementary information (SI). Supplementary information is available. See DOI: https://doi.org/10.1039/d6py00380j.

Additional raw data is available from the corresponding author upon reasonable request.

Acknowledgements

We acknowledge the financial support received from CONICET (11220200101353CO), CONICET (28720210100098CO), UNL (CAID 85520240100107LI) and ANPCyT (PICT-2019-01265) from Argentina, and Marie Skłodowska-Curie Actions Staff Exchanges under grant agreement no. 101129945, "IONBIKE 2.0." The authors acknowledge the financial support received from the IKUR Strategy 2022 (Nanoneuro).

References

1 U. A. Weerasinghe, T. Wu, P. L. Chee, P. Y. M. Yew, H. K. Lee, X. J. Loh and K. Dan, *Green Chem.*, 2024, **26**, 8497–8527, DOI: 10.1039/d4gc00532e.
2 P. A. Mercadal, A. González, A. Beloqui, L. C. Tomé, D. Mecerreyes, M. Calderón and M. L. Picchio, *JACS Au*, 2024, **4**, 3744–3758, DOI: 10.1021/jacsau.4c00677.
3 A. Nicolau, A. L. Mutch and S. C. Thickett, *Macromol. Rapid Commun.*, 2024, **45**, 2400405, DOI: 10.1002/marc.202400405.
4 T. Zhou, H. Yuk, F. Hu, J. Wu, F. Tian, H. Roh, Z. Shen, G. Gu, J. Xu, B. Lu and X. Zhao, *Nat. Mater.*, 2023, **22**, 895–902, DOI: 10.1038/s41563-023-01569-2.
5 S. J. Lee, T. Esworthy, S. Stake, S. Miao, Y. Y. Zuo, B. T. Harris and L. G. Zhang, *Adv. Biosyst.*, 2018, **2**, 1700213, DOI: 10.1002/adbi.201700213.
6 R. J. Mondschein, A. Kanitkar, C. B. Williams, S. S. Verbridge and T. E. Long, *Biomaterials*, 2017, **140**, 170–188, DOI: 10.1016/j.biomaterials.2017.06.005.
7 J. L. de Lacalle, M. L. Picchio, A. Dominguez-Alfaro, R. R. M. Serrano, B. Marchiori, I. del Agua, N. Lopez-Larrea, M. Criado-Gonzalez, G. G. Malliaras and D. Mecerreyes, *ACS Mater. Lett.*, 2023, **5**, 3340–3346, DOI: 10.1021/acsmaterialslett.3c00938.
8 R. R. M. Serrano, A. Aguzin, E. Mitoudi-Vagourdi, X. Tao, T. E. Naegele, A. T. Jin, N. Lopez-Larrea, M. L. Picchio, M. V. Alban-Paccha, R. J. Minari, D. Mecerreyes, A. Dominguez-Alfaro and G. G. Malliaras, *Biomaterials*, 2024, **310**, 122624, DOI: 10.1016/j.biomaterials.2024.122624.
9 S. Marullo, F. Petta, G. Infurna, N. T. Dintcheva and F. D'Anna, *Green Chem.*, 2023, **25**, 4513–4527, DOI: 10.1039/d3gc00573a.
10 S. Locatelli, G. C. Luque, R. R. M. Serrano, A. Dominguez-Alfaro, G. Reniero, M. L. Picchio, J. Leiva, L. M. Gugliotta, G. G. Malliaras, D. Mecerreyes, L. I. Ronco and R. J. Minari, *ACS Appl. Polym. Mater.*, 2025, **7**, 2945–2954, DOI: 10.1021/acsapm.4c03592.
11 G. Yusakul, J. Jomrit, R. G. Bacabac and A. Prasopthum, *RSC Adv.*, 2024, **14**, 34175–34191, DOI: 10.1039/d4ra05456c.
12 K. Parkatzidis, M. Chatzinikolaidou, M. Kaliva, A. Bakopoulou, M. Farsari and M. Vamvakaki, *ACS Biomater. Sci. Eng.*, 2019, **5**, 6161–6170, DOI: 10.1021/acsbiomaterials.9b01300.
13 I. Chiulan, E. B. Heggset, Ş. I. Voicu and G. Chinga-Carrasco, *Biomacromolecules*, 2021, **22**, 1795–1814, DOI: 10.1021/acs.biomac.0c01745.
14 P. N. Bernal, S. Florczak, S. Inacker, X. Kuang, J. Madrid-Wolff, M. Regehly, S. Hecht, Y. S. Zhang, C. Moser and R. Levato, *Nat. Rev. Mater.*, 2025, **10**, 826–841, DOI: 10.1038/s41578-025-00785-3.
15 J. T. Toombs, M. Luitz, C. C. Cook, S. Jenne, C. C. Li, B. E. Rapp, F. Kotz-Helmer and H. K. Taylor, *Science*, 2022, **376**, 308–312, DOI: 10.1126/science.abm6459.
16 F. M. Fuad and M. M. Nadzir, *J. Mol. Liq.*, 2022, **360**, 119392, DOI: 10.1016/j.molliq.2022.119392.
17 D. Shin and J. Hyun, *J. Ind. Eng. Chem.*, 2021, **95**, 126–133, DOI: 10.1016/j.jiec.2020.12.011.
18 X. Mu, J. K. Sahoo, P. Cebe and D. L. Kaplan, *Polymers*, 2020, **12**, 2936, DOI: 10.3390/polym12122936.
19 M. B. Applegate, B. P. Partlow, J. Coburn, B. Marelli, C. Pirie, R. Pineda, D. L. Kaplan and F. G. Omenetto, *Adv. Mater.*, 2016, **28**, 2417–2420, DOI: 10.1002/adma.201504527.
20 S. G. Bertolotti, C. M. Previtali, A. M. Rufs and M. V. Encinas, *Macromolecules*, 1999, **32**, 2920–2924, DOI: 10.1021/ma981246f.
21 J. W. Stansbury and S. H. Dickens, *Dent. Mater.*, 2001, **17**, 71–79, DOI: 10.1016/S0109-5641(00)00062-2.
22 A. Gallastegui, A. Dominguez-Alfaro, L. Lezama, N. Alegret, M. Prato, M. L. Gómez and D. Mecerreyes, *ACS Macro Lett.*, 2022, **11**, 303–309, DOI: 10.1021/acsmacrolett.1c00758.

23 H. J. Hageman, *Prog. Org. Coat.*, 1985, **13**, 123–150, DOI: 10.1016/0033-0655(85)80021-2.
24 X. Hou, T. P. Pollard, X. He, L. Du, X. Ju, W. Zhao, M. Li, J. Wang, E. Paillard, H. Lin, J. Sun, K. Xu, O. Borodin, M. Winter and J. Li, *Adv. Energy Mater.*, 2022, **12**, 2200401, DOI: 10.1002/aenm.202200401.
25 H. Monteiro, A. Paiva, A. R. C. Duarte and N. Galamba, *Phys. Chem. Chem. Phys.*, 2023, **25**, 439–454, DOI: 10.1039/D2CP04139A.
26 A. Jastram, J. Claus, P. A. Janmey and U. Kragl, *Polym. Test.*, 2021, **93**, 106943, DOI: 10.1016/j.polymertesting.2020.106943.
27 E. Nikoumanesh, C. J. M. Jouaneh and R. Poling-Skutvik, *Soft Matter*, 2024, **20**, 7094–7102, DOI: 10.1039/d4sm00516c.
28 H. Xia, M. Ren, Y. Zou, S. Qin and C. Zeng, *Molecules*, 2020, **25**, 3314, DOI: 10.3390/molecules25153314.
29 P. M. De Molina, S. Lad and M. E. Helgeson, *Macromolecules*, 2015, **48**, 5402–5411, DOI: 10.1021/acs.macromol.5b01115.
30 R. Vo, H. H. Hsu and X. Jiang, *Biomater. Sci.*, 2021, **9**, 23–37, DOI: 10.1039/d0bm01373k.
31 C. T. McKee, J. A. Last, P. Russell and C. J. Murphy, *Tissue Eng., Part B*, 2011, **17**, 155–164, DOI: 10.1089/ten.teb.2010.0520.
32 H. Yuk, B. Lu and X. Zhao, *Chem. Soc. Rev.*, 2019, **48**, 1642–1667, DOI: 10.1039/c8cs00595h.
33 S. Zhuo, C. Song, Q. Rong, T. Zhao and M. Liu, *Nat. Commun.*, 2022, **13**, 1743, DOI: 10.1038/s41467-022-29424-z.
34 Z. Huang, L. Xu, P. Liu and J. Peng, *RSC Adv.*, 2024, **14**, 28234–28243, DOI: 10.1039/d4ra05446f.
35 S. Nechausov and A. Miriyev, *Chem. Eng. J.*, 2024, **496**, 153759, DOI: 10.1016/j.cej.2024.153759.
36 M. L. Picchio, A. Gallastegui, N. Casado, N. Lopez-Larrea, B. Marchiori, I. del Agua, M. Criado-Gonzalez, D. Mantione, R. J. Minari and D. Mecerreyes, *Adv. Mater. Technol.*, 2022, **7**, 2101680, DOI: 10.1002/admt.202101680.
37 G. Li, Z. Deng, M. Cai, K. Huang, M. Guo, P. Zhang, X. Hou, Y. Zhang, Y. Wang, Y. Wang, X. Wu and C. F. Guo, *npj Flexible Electron.*, 2021, **5**, 23, DOI: 10.1038/s41528-021-00118-8.
38 Z. Huang, J. Xie, T. Li, L. Xu, P. Liu and J. Peng, *Polymers*, 2024, **16**, 2761, DOI: 10.3390/polym16192761.
39 Q. Quan, C. Fan, N. Pan, M. Zhu, T. Zhang, Z. Wang, Y. Dong, Y. Wu, M. Tang, X. Zhou and M. Chen, *Adv. Funct. Mater.*, 2023, **33**, 2303381, DOI: 10.1002/adfm.202303381.
40 Z. Ma, J. Zhang, Z. Ma, M. Lou, P. Zou, H. Wang and L. Jia, *J. Mater. Chem. A*, 2025, **13**, 9418–9427, DOI: 10.1039/d5ta00422e.
41 E. Sanchez-Rexach, P. T. Smith, A. Gomez-Lopez, M. Fernandez, A. L. Cortajarena, H. Sardon and A. Nelson, *ACS Appl. Mater. Interfaces*, 2021, **13**, 19193–19199, DOI: 10.1021/acsami.0c22377.
42 P. T. Smith, B. Narupai, J. H. Tsui, S. C. Millik, R. T. Shafranek, D. H. Kim and A. Nelson, *Biomacromolecules*, 2020, **21**, 484–492, DOI: 10.1021/acs.biomac.9b01236.
43 B. D. Fairbanks, M. P. Schwartz, C. N. Bowman and K. S. Anseth, *Biomaterials*, 2009, **30**, 6702–6707, DOI: 10.1016/j.biomaterials.2009.08.055.
44 A. K. Nguyen, P. L. Goering, V. Reipa and R. J. Narayan, *Biointerphases*, 2019, **14**, 021007, DOI: 10.1116/1.5095886.